# Method for evaluating the health risk in urban pedestrian space in extremely hot summer conditions based on the total analysis of mesoscale and microscale climates

Saori Yumino[1], Akashi Mochida[1], Naohiro Hamada[2], Susumu Ohno[3]

[1] *Tohoku University, #1206 6-6-11 Aoba Aramaki-Aza Aoba-ku Sendai, Japan, yumino@sabine.pln.archi.tohoku.ac.jp, mochida@sabine.pln.archi.tohoku.ac.jp*

[2] *Mitsubishi Jisho Sekkei Inc., 2-5-1, Marunouchi, Chiyoda-ku, Tokyo, Japan*

[3] *Tohoku University, 468-1 Aoba Aramaki-Aza Aoba-ku Sendai, Japan, ohnos@saigai.str.archi.tohoku.ac.jp*

dated : 15 June 2015

## 1. Introduction

Health hazards of extremely hot summer conditions (e.g., heatstroke) have increased rapidly in recent years with issues such as urban heat island and severe weather. In this study, the increase in the number of heatstroke patients caused by extremely hot summer conditions was regarded as a disaster, and a new evaluation method for outdoor thermal environment based on the concept of risk evaluation was developed.

## 2. Concept of risk evaluation method

### 2.1 Formulation of health hazard risk

Commonly, a risk that the society is exposed to when it is struck by disaster is defined as follows.

$$Risk = Magnitude\ of\ hazard \times Intensity\ of\ influence\ on\ society = f(Hazard) \quad (1)$$

$f$ : a function that expresses the relationship between hazard and risk.

This study is focused on health hazards in extremely hot conditions. Therefore, the emergency transport ratio for heatstroke and the thermal index that indicates the severity of the thermal environment related to the occurrence of heatstroke were selected as variables to represent the risk and the hazard, respectively, and the emergency transport probability curve was used as a function to represent the relationship between the hazard and the risk in this study.

### 2.2 Definition of hazard in this study

The thermal environment inside an urban area is formed by a combined influence of weather conditions above the urban area and urban structure, e.g., the building shape and arrangement, the green cover ratio, the intensity of anthropogenic heat release, and so on. Inside an urban area, the thermal environment is often severer than that above it owing to the effect of the urban structure (Fig. 1). In other words, inappropriate urban planning and building design can amplify threats caused by weather conditions above an urban area. In this study, to distinguish between hazards that cannot be controlled by humans and those that can be controlled by modification of urban structures, “natural hazard” and “actual hazard” were defined, respectively. Specifically, a natural hazard is an uncontrollable hazard, which can be estimated from weather conditions above an urban area, while an actual hazard is a hazard that pedestrians are exposed to because of the thermal environment inside the urban area. A “hazard increment” is a component of hazard and is the increase in threat caused by inappropriate urban planning and building design. An actual hazard is a combination of a natural hazard and hazard increment.

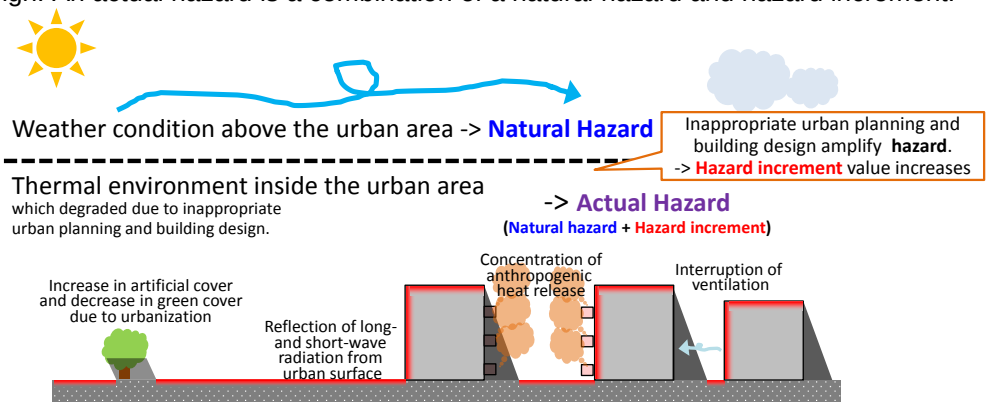


*Fig.1 Concept of risk evaluation*

### 2.3 Index of vulnerability of urban structures based on risk evaluation

The risk above an urban area, $R_{above}$, and that inside the urban area, $R_{inside}$, can be estimated from the values of natural and actual hazards, respectively.

$$R_{above} = f(Natural\ hazard) \quad (2)$$
$$R_{inside} = f(Actual\ hazard) \quad (3)$$

Dividing formula (3) by (2), we get

$$R_{inside} / R_{above} = f(Actual\ hazard) / f(Natural\ hazard) \quad (4)$$

Right hand side of formula (4) is defined as risk amplification ratio in this study. This ratio is an index that comprehends the increase in health risks caused by amplification of hazards inside an urban area because of inappropriate urban planning and design. By transposing the denominator of the left hand side in (4), $R_{inside}$ can be expressed as:

$$R_{inside} = R_{above} \times Risk\ amplification\ ratio \quad (5)$$

Formula (5) indicates that the risk amplification ratio shows thermal vulnerability borne by the urban area (Belcher, 2012). If the ratio exceeds 1, it means that the urban structure amplifies health risks, and if it is less than 1, the urban structure reduces health risks.

## 3. Estimation of emergency transport probability curves for heatstroke based on emergency transport data analysis

From the comparison between emergency transport data and meteorological data, a thermal index that is strongly linked to the increase in the number of occurrence of heatstroke was investigated.

### 3.1 Outline of emergency transport data

Each emergency transport data unit contains information about the injury and disease, date and time of occurrence, patient's age, patient's sex, site of occurrence, and symptom severity. Data on heatstroke extracted from five years' emergency transport data from 2008 to 2012 were provided by fire departments located in nine major cities of Japan: Sendai, Tokyo, Yokohama, Shizuoka, Hamamatsu, Nagoya, Osaka, Kobe, and Fukuoka. Table 1 shows the number of samples in each city.

### 3.2 Outline of meteorological observatory data

In this study, air temperature and wet bulb globe temperature (WBGT) were compared with the number of occurrence of heatstroke. WBGT was estimated from following equation:

$$WBGT = 0.7T_w + 0.2T_g + 0.1T_a \quad (6)$$

$T_w$ : Wet bulb temperature [K]
$T_g$ : Globe temperature [K]
$T_a$ : Air temperature [K]

WBGT was estimated from air temperature, absolute humidity, and atmospheric pressure, and the method of estimating wet bulb temperature was identical to that proposed by the Ministry of the Environment, Government of Japan (2010). The globe temperature was estimated from the amount of global solar radiation, wind velocity, and air temperature. Observation values of air temperature, absolute humidity, atmospheric pressure, solar radiation, and wind velocity were obtained from data provided by meteorological observatories in each city.

*Table 1 Number of data samples in each city*

| | City | Patients |
|---|---|---|
| Number of occurrences of emergency transport | Sendai | 1,268 |
| | Tokyo | 7,615 |
| | Yokohama | 2,074 |
| | Shizuoka | 584 |
| | Hamamatsu | 794 |
| | Nagoya | 4,418 |
| | Osaka | 3,160 |
| | Kobe | 1,800 |
| | Fukuoka | 1,495 |

*Table 2 Thresholds values of WBGT in each city*

| City | Average air temperature in the summer season | Threshold of daily average air temperature | Threshold of the daily average of WBGT |
|---|---|---|---|
| Sendai | 20 | 28 | 26 |
| Yokohama | 23 | 29 | 27 |
| Hamamatsu | 24 | 29 | 28 |
| Shizuoka | 24 | 31 | 27 |
| Tokyo | 24 | 32 | 28 |
| Nagoya | 24 | 32 | 27 |
| Fukuoka | 25 | 31 | 28 |
| Kobe | 25 | 30 | 28 |
| Osaka | 25 | 32 | 28 |

### 3.2 Analysis results

Figs. 2 and 3 show the relationship between the emergency transport ratio and the two thermal indices air temperature and WBGT. WBGT correlated with the number of heatstroke patients more clearly than air temperature. Therefore, the relationship between WBGT and the emergency transport ratio was defined as the emergency transport probability curve in this study.

In addition, thresholds of air temperature and WBGT for rapid increases in heatstroke patients were estimated. Table 2 shows the threshold values of air temperature and WBGT in each city. The thresholds in Sendai, located in the northern part of Japan, were higher than those in other cities.

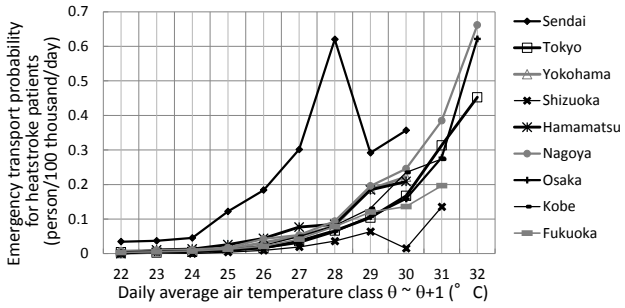


*Fig. 2 Relationship between the daily-averaged air temperature and emergency transport ratio*

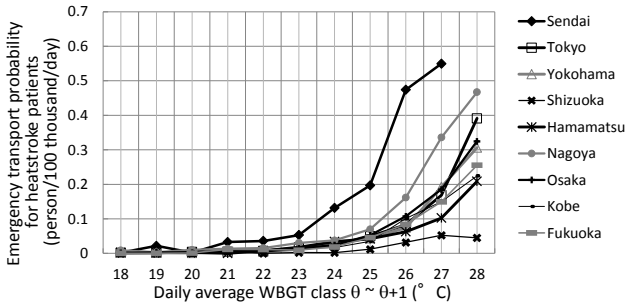


*Fig. 3 Relationship between the daily-averaged WBGT and emergency transport ratio*

*Table 3 Ranking of the daily number of occurrence of emergency transport for heatstroke in Sendai City*

| Rank | Date | Patients |
|---|---|---|
| 1 | 2011/07/16 | 20 |
| 2 | 2012/07/28 | 16 |
| 3 | 2010/07/24 | 15 |
| 4 | 2010/07/22 | 13 |
| 5 | 2012/07/29 | 12 |
| 6 | 2010/08/05 | 11 |
| 7 | 2010/08/08 | 10 |
| 8 | 2010/08/07 | 9 |
| 9 | 2011/07/17 | 9 |
| 10 | 2010/08/06 | 8 |

*Table 4 Size of the computational domain and numb WRF simulation mesh*

| | Domain size (X×Y) [km$^2$] | Grid arrangement (I×J×K) | Grid size (X×Y) [km$^2$] |
|---|---|---|---|
| Domain 1 | 1800×1800 | 72×72×44 | 25×25 |
| Domain 2 | 500×500 | 100×100×44 | 5×5 |
| Domain 3 | 120×120 | 120×120×44 | 1×1 |

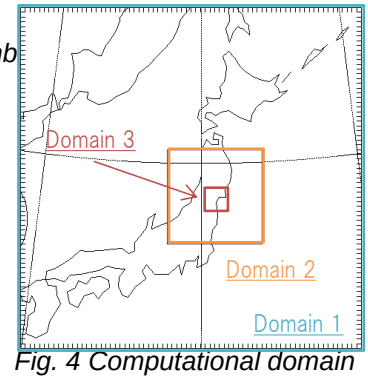


*Fig. 4 Computational domain of WRF simulation*

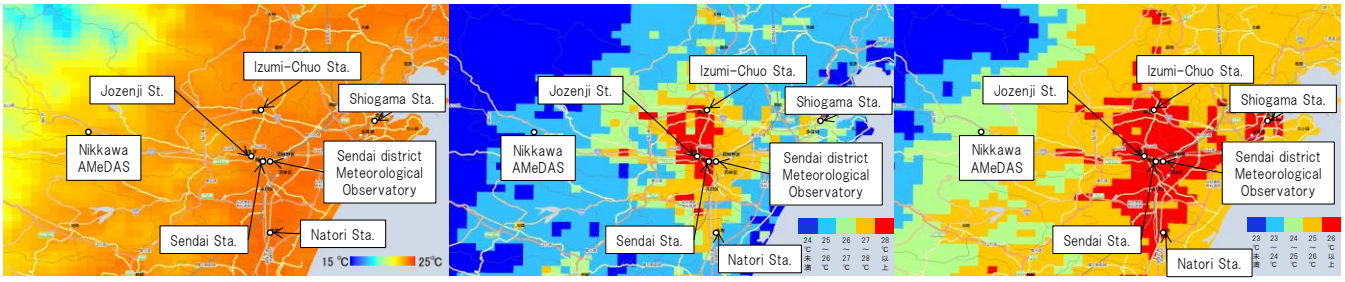


(1) Wet bulb temperature (2) Dry bulb temperature (3) WBGT

*Fig. 5 Spatial distribution of thermal indices estimated from the WRF simulation (average of 10 days (Table 3), at a height of 2 m)*

## 4. Application of the risk evaluation method

In this section, the urban environment in Sendai city is assessed using the risk evaluation method proposed in this study as an example.

### 4.1 Extraction of at-risk area based on mesoscale climate analysis

#### 4.1.1 Calculation conditions for a mesoscale climate analysis

The calculation periods were a total of four months including the days when the daily number of occurrences of emergency transport for heatstroke was in the top ten (Table 3). An analysis of at-risk area was performed for these ten days. As shown in Fig. 4, three nested domains were used. The sizes of the computational domains and the mesh numbers are listed in Table 4. The Weather Research and Forecasting (WRF) modeling system (version 3.2.1), equipped with an ARW (Advanced Research WRF) dynamics solver, was used. Calculation conditions for a mesoscale climate analysis are described in Yumino et al. (2014).

#### 4.1.2 Calculation results

The spatial distributions of the average wet bulb temperature, air temperature, and WBGT for the ten days are shown in Fig. 5. The methods for estimating the wet bulb temperature, globe temperature, and WBGT were the

same as those described in Section 3.2. The red zones in Figs. 5(2) and (3) are the areas where the air temperature or WBGT value exceeds the threshold. The spatial distribution of WBGT in Fig. 5 (3) shows a red zone larger than the area showing the spatial distribution of air temperature (Fig. 5 (1)); this is due to the effect of wet bulb temperature. The difference between wet bulb temperatures in urban and coastal areas was smaller than that between air temperatures in these areas.

In the next section, risk evaluation is discussed for the central region of Sendai located in the red zone in Fig. 5 (3). The analysis date was July 16, 2011 when the number of instances of emergency transport for heat stroke was the highest. The value of WBGT above urban areas, which indicates the natural hazard value, was 26.5 °C at 12 p.m. on July 16, 2011. The change in the actual hazard value by the hazard increment due to urban structure will be estimated in the next section.

### 4.2 Evaluation of hazard distribution in pedestrian spaces through a combined analysis of mesoscale and microscale climates

#### 4.2.1 Calculation conditions for the microscale climate analysis

A microscale climate analysis using the results of the mesoscale climate analysis as boundary conditions was performed. The calculation conditions for the microscale climate analysis are described in Yumino et al. (2014). The time selected for calculation is 12 p.m. on July 16, 2011. The simulation target was Jozenji Street located in the central region of Sendai, and the computation domain is shown in Fig. 6, Photo 1, and Table 5. Zelkova trees that were about 15 m high are planted on the sides of the roads for over 700 m on Jozenji Street. Two situations were simulated to investigate the effect of the roadside trees on changes in actual hazard values inside the urban area: one is the case with roadside trees, and the other is without roadside trees.

#### 4.2.2 Calculation results

**(1) Mean radiant temperature (MRT)**

The horizontal distributions of MRT at a height of 1.25 m are illustrated in Fig. 7. MRT in the case with roadside trees was lower than that in the case without roadside trees notably in the eastern region of the computational domain that is covered with roadside trees.

**(2) Wind velocity**

The horizontal distributions of wind velocity are shown in Fig. 8. High–wind-speed areas extended from southeast to northwest in the computational domain in both cases.

**(3) WBGT**

Fig. 9 shows a comparison of the horizontal distributions of WBGT, which represents the actual hazard values inside the urban area. In this calculation, the globe temperature was estimated by using the equation proposed by ASHRAE (2013) for calculating the MRT from the globe temperature. WBGT in the case with roadside trees was lower than that in the case without roadside trees. This is because the shade provided by roadside trees reduced the WBGT.

### 4.3 Risk evaluation results

Table 6 shows the results of the risk evaluation discussed in this section. The risk amplification ratio was reduced from 1.2 to 0.6 in the case with roadside trees, indicating that roadside trees reduced the risk considerably owing to the shade provided by roadside trees under the conditions assumed in this study.

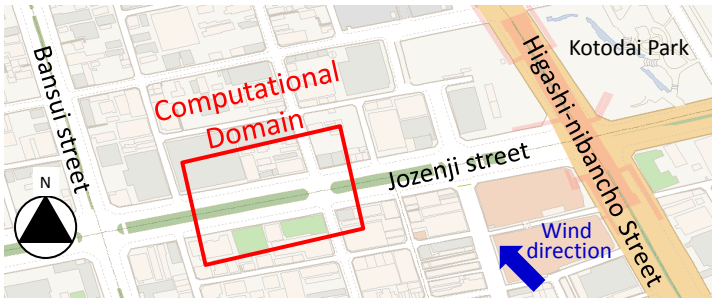


*Fig. 6 Computational domain of microscale simulation*

*Photo 1 Jozenji Street (Simulation target)*

*Table 5 Size of the computational domain and mesh numbers of microscale simulation*

| | Coupled simulation of radiation and conduction | Isothermal CFD simulation |
|---|---|---|
| Computational domain (X[m]×Y[m]×Z[m]) | 32×27×18 | 69×65×52 |
| Grid arrangement (I×J×K) | 340×300×200 | 171×151×550 |
| Mesh number | 15552 | 233220 |

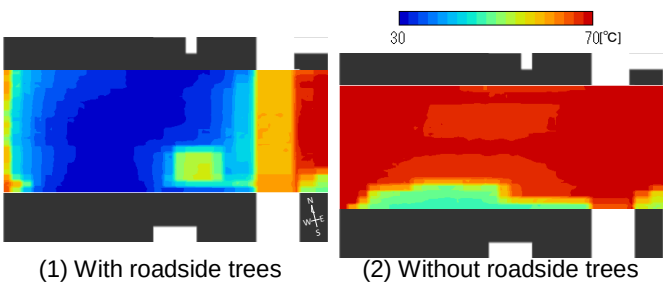


(1) With roadside trees (2) Without roadside trees

*Fig. 7 Horizontal distributions of MRT (at a height of 1.15 m)*

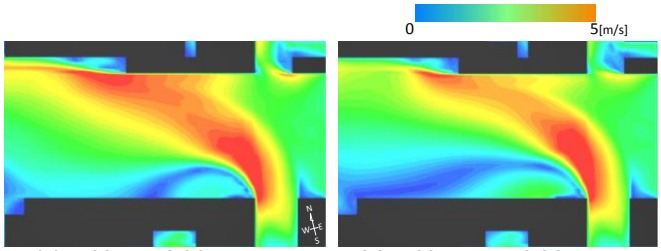


(1) With roadside trees (2) Without roadside trees

*Fig. 8 Horizontal distributions of wind velocity (at a height of 1.15 m)*

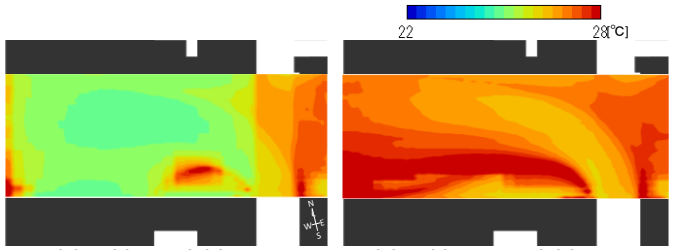


(1) With roadside trees (2) Without roadside trees

*Fig. 9 Horizontal distributions of WBGT (at a height of 1.15 m)*

*Table 6 Results of risk evaluation*

| | ***Natural Hazard*** WBGT value estimated from weather condition above urban area [°C] | ***Actual Hazard*** Average WBGT over pedestrian space [°C] | ***Hazard increment*** Difference between Natural Hazard and Actual Hazard [°C] |
|---|---|---|---|
| With roadside trees | 26.5 | 25.6 | - 0.9 |
| Without roadside trees | | 26.9 | + 0.4 |
| | **f(*Natural Hazard*)** Risk value estimated from Natural Hazard [person/100 thousand people/day] | ***f*(Actual Hazard)** Risk value estimated from Actual Hazard [person/100 thousand people/day] | ***Risk amplification ratio*** [-] |
| With roadside trees | 0.36 | 0.22 | 0.62 |
| Without roadside trees | | 0.43 | 1.2 |

## 5. Conclusions

1) The increase in the number of heatstroke patients caused by extremely hot summer conditions was regarded as a disaster, and a new method for evaluating the outdoor thermal environment based on the concept of risk evaluation was developed.
2) Emergency transport probability curves for nine cities were estimated based on a comparison between emergency transport data and meteorological data.
3) The spatial distribution of actual hazard values inside urban areas and the health risk value were estimated from the results of a microscale climate analysis using the result of a mesoscale climate analysis as boundary conditions for the central region of Sendai. Roadside trees reduced the health risk by providing shade under the conditions assumed in this study.
4) The results obtained in this study are based on preliminary trials that introduce the concept of risk evaluation in urban planning. Further discussion is required to evaluate risks more effectively.

## Acknowledgment

This work was supported by a JSPS Grant-in-Aid for Scientific Research (B) (Grant Number 26289200), and a Grant-in-Aid for JSPS Fellows. The authors wish to thank the fire departments of Sendai, Tokyo, Yokohama, Shizuoka, Hamamatsu, Nagoya, Osaka, Kobe, and Fukuoka for providing emergency transport data.

## References

ASHRAE, 2013. ASHRAE Handbook Fundamentals. Atlanta

Belcher S., 2012. Cities and Climate change. Plenary Lecture at 8th International Conference on Urban Climate, Dublin

Ministry of the Environment in Japan, 2010. Report on provision affair of information on prevention of heatstroke based on WBGT observation

Yumino S., Tsubasa O., Mochida A., 2014. Prediction of microclimate around buildings based on CFD and heat balance analysis using WRF results as boundary conditions to include topographic influences. *Proceedings of Computational Wind Engineering*